9-2012

Characterization of structure and function of the mouse retina using pattern electroretinography, pupil light reflex, and optical coherence tomography

Kabhilan Mohan
Iowa State University

Matthew M. Harper
United States Department of Veterans Affairs

Helga Kecova
United States Department of Veterans Affairs

Eun-Ah Ye
Iowa State University

Jana Lazic
United States Department of Veterans Affairs

See next page for additional authors

Veterinary Ophthalmology (2012) **15**, Supplement 2, 94–104 DOI:10.1111/j.1463-5224.2012.01034.x

Characterization of structure and function of the mouse retina using pattern electroretinography, pupil light reflex, and optical coherence tomography

Kabhilan Mohan,*,† Matthew M. Harper,* Helga Kecova,* Eun-Ah Ye,‡ Tatjana Lazic,* Donald S. Sakaguchi,*,‡ Randy H. Kardon*,§ and Sinisa D. Grozdanic¶ CR: BioMed Vision Technologies, Neuroptics Inc.

**Iowa City Department of Veterans Affairs Center for Prevention and Treatment of Vision Loss, Iowa City, IA 52246-2209, USA; †Department of Biomedical Sciences, Iowa State University, Ames, IA, USA; ‡Genetics Development and Cell Biology, Iowa State University, Ames, IA, USA; §Department of Ophthalmology and Visual Sciences, University of Iowa, Iowa City, IA, USA; and ¶Eastern Iowa Veterinary Specialty Center, Cedar Rapids, IA 52404, USA*

Address communications to:
M. Harper and S. Grozdanic
Tel.: (319) 339-7151
Fax: (319) 887-4993
e-mails: matthew.harper@va.gov, sgrozdan@gmail.com

Abstract

Objective To perform *in vivo* analysis of retinal functional and structural parameters in healthy mouse eyes.

Animal Studied Adult C57BL/6 male mice (n = 37).

Procedures Retinal function was evaluated using pattern electroretinography (pERG) and the chromatic pupil light reflex (cPLR). Structural properties of the retina and nerve fiber layer (NFL) were evaluated using spectral-domain optical coherence tomography (SD-OCT).

Results The average pERG amplitudes were found to be 11.2 ± 0.7 μV (P50-N95, mean ± SEM), with an implicit time for P50-N95 interval of 90.4 ± 5.4 ms. Total retinal thickness was 229.5 ± 1.7 μm (mean ± SEM) in the *area centralis* region. The thickness of the retinal nerve fiber layer (mean ± SEM) using a circular peripapillary retinal scan centered on the optic nerve was 46.7 ± 0.9 μm (temporal), 46.1 ± 0.9 μm (superior), 45.8 ± 0.9 μm (nasal), and 48.4 ± 1 μm (inferior). The baseline pupil diameter was 2.1 ± 0.05 mm in darkness, and 1.1 ± 0.05 and 0.56 ± 0.03 mm after stimulation with red (630 nm, luminance 200 kcd/m^2) or blue (480 nm, luminance 200 kcd/m^2) light illumination, respectively.

Conclusions Pattern electroretinography, cPLR and SD-OCT analysis are reproducible techniques, which can provide important information about retinal and optic nerve function and structure in mice.

Key Words: mouse, OCT, pERG, pupil, retina

INTRODUCTION

Noninvasive functional and structural assays such as electroretinography (ERG) and optical coherence tomography (OCT) can be utilized in animal models to obtain objective information regarding the status of the retina and optic nerve *in vivo*.[1–3] These techniques allow repeated analysis without the need to euthanize the animal and can be effectively used for longitudinal evaluation of disease progression or treatment efficacy. The function of retinal ganglion cells (RGCs) in rodents can be measured by recording the amplitude and latency of the pattern-evoked electroretinogram (pERG).[4–12] The pERG response is a result of RGCs depolarization[13,14] with minimal glial cell contributions,[15] which can be abolished by optic nerve transection[16,17] or pharmacological blockade targeting RGC action potential activity.[13] Considering that the electrical response originates from RGCs, pERG has been used to evaluate RGC damage associated with glaucoma and ocular hypertension in human patients[18–20] and in different animal models.[21–23]

The chromatic pupil light response (cPLR) analysis is a relatively new diagnostic technique, which may provide information about the quality of rod-cone activity, rod-cone-mediated electrical signal transmission to RGCs and characteristics of an intrinsically photosensitive subpopulation of RGCs (ipRGCs) containing the pigment

melanopsin.[24–30] Recent reviews have excellently described the anatomy of ipRGCs and have summarized their role in mediating various functional properties.[31–34] Stimulation of the retina with red (630 nm) light activates strictly rod-cone-mediated pupil light response, without activation of melanopsin-mediated responses.[24] The degree of contribution of rods vs. cones depends on the state of retinal adaptation, the spectral sensitivity of the photoreceptors in the species being studied, and the brightness of the light. The rod-cone-mediated pupil response requires six components: (i) normal functioning rods and cones and their respective neurons in the inner nuclear layer, (ii) functional and well-organized dendritic arborization of ipRGCs to allow for a rod-cone generated electrical response to be transmitted to the ipRGCs that results in a generation of PLR responses, (iii) functional axons of ipRGCs to transmit the electrical information to the pretectal brain regions mediating the PLR and photopic blink responses, (iv) normal status of the pretectal olivary nucleus as a brain interneuron relay station for mediating the PLR to both Edinger-Westphal Nuclei, (v) intact pre- and post-ganglionic parasympathetic nerve pathway (oculomotor nerve) as an efferent pathway for mediation of PLR response, and (vi) an intact iris sphincter as an effector organ. Stimulation of the retina with bright blue (480 nm) light can activate both a rod-cone-mediated pupil response and a pupil response that is elicited by activation of the melanopsin in ipRGCs.[3,25,35–37] However, the melanopsin activated pupil response is typically more sustained after light termination.

Spectral-domain optical coherence tomography (SD-OCT) is a high-resolution imaging technique used for direct *in vivo* analysis of retina and optic nerve head structure.[38–40] Recent studies have demonstrated that OCT analysis of retinal thickness provides nearly identical values compared with analysis of the same retinal regions using position-matched histological analysis.[41] Different OCT segmentation protocols allow for the measurement of total retina thickness, photoreceptor layer thickness, and thickness of the retinal nerve fiber layer (RNFL) in different retinal quadrants.[42–46] Recent utilization of OCT technology in rodent models of eye diseases has provided an objective measure of retinal structure, which can be used to monitor the structural effects of disease progression or treatment response.[45–49]

The principal objective of this study was to perform a detailed characterization of RGC functional and structural parameters with the goal of establishing normative data for adult healthy C57BL/6 mice as a basis for further investigations by us and others on the experimental effects of retinal and optic nerve disorders and their treatment. In this study, we used pERG and cPLR analyses to evaluate the retinal function, and particularly RGC function, while SD-OCT was used to provide structural information about the retina, photoreceptor layer, and RNFL thickness.

MATERIALS AND METHODS

Animals

All animal studies were conducted in accordance with the ARVO Statement for the Use of Animals in Ophthalmic and Vision Research and had the approval of the Iowa State University and VA Medical Center-Iowa City Institutional Animal Care and Use Committees. A total of 37 adult healthy male C57BL/6 mice (8–12 weeks of age, unless otherwise specified) were used for the purpose of this study.

Pattern electroretinography

Pattern-evoked electroretinography (pERG) was used to objectively measure the function of the RGCs by recording the amplitude and latency of the pERG waveform. Mice (n = 37) were anesthetized with 0.8 L/min O_2, 0.4 L/min nitrous oxide, and 3.5% halothane. After anesthesia induction, the halothane concentration was decreased to 1.75% and mice were placed on a stainless steel recording table equipped with an internal circulating hot-water-based warming system (maintained at 39 °C) to maintain body temperature. The mice were positioned 20 cm from the stimulus monitor with their body angle tilted at 45 degrees to provide direct exposure of the stimulus to the visual axis of the recorded eye. The pupil was then dilated using 1% tropicamide solution (Tropicamide; Falcon Pharmaceuticals, Fort Worth, TX, USA). Pattern ERG responses were evoked using alternating, reversing, black and white vertical stimuli delivered on a monitor (Fig. 1a) with a Roland Consult ERG system (Roland Consult, Brandenburg, Germany). To record the pERG response, commercially available mouse corneal gold ring electrodes were used (S&V Technologies AG, Hennigsdorf, Germany). A reference needle electrode was placed at the base of the head, and a ground electrode was placed at the base of the tail to complete the circuit. Each animal was placed at the same fixed position in front of the monitor to prevent recording variability because of animal placement. Stimuli (9° radius visual angle subtended on full field pattern, 1 Hz temporal frequency, 0.05 cycles/deg spatial frequency, 97% contrast, 80 cd/m^2 monitor luminance, and 200 averaged signals with cut-off filter frequencies of 1–30 Hz) were delivered under photopic conditions, because slower stimulation rates in mesopic and scotopic conditions can elicit rod-mediated full field ERG responses, which can completely conceal the pERG response. Retinal pERG responses were evaluated by measuring the amplitudes (N35-P50 and P50-N95) and respective implicit times (Fig. 2). Implicit times were calculated for N35, P50, and N95 markers, in addition to the implicit time for N35-P50 and P50-N95 components. Seven mice were repeatedly recorded at 3, 11, and 15 months of age to determine whether aging has any effect on pERG amplitudes or implicit times.

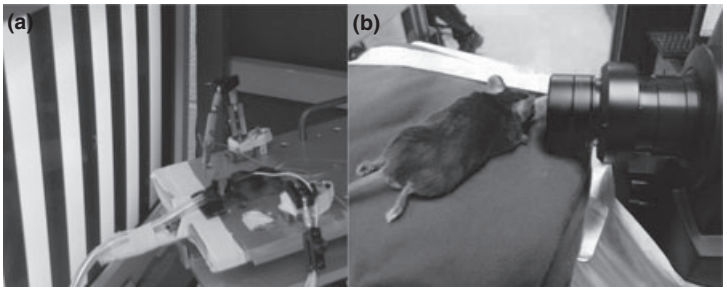

Figure 1. (a) Pattern ERG recording in mice. The mouse is positioned on a heated table and placed 20 cm from the stimulating screen. The position of the table and eye orientation is carefully controlled to provide consistent placement of the animal eye in front of the stimulating monitor. (b) Optical coherence tomography (OCT) recording in mice. A special 25D lens is attached to the spectral-domain optical coherence tomography Spectralis system for performing OCT imaging in mouse eyes. Anesthetized mice are kept warm by placement on a heating pad for the duration of the recording.

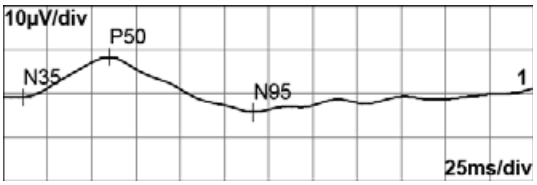

Figure 2. Representative mouse pattern electroretinography tracing. Amplitudes are calculated for N35-P50 and P50-N95 intervals. It is considered that P50-N95 amplitude represents electrical activity of the retinal ganglion cell body and dendritic tree as a result of cell membrane depolarization.

Chromatic pupillography

Chromatic pupil light reflex (PLR) was characterized in mice (n = 8) using the A2000 COMPUTERIZED PUPILLOMETER (Neuroptics, San Clemente, CA, USA). The pupillometer consists of a sensitive pupil tracking software, which can be programmed to include various PLR recording routines and can provide the required red/blue light illumination. Red light of 630 nm was used to elicit strictly rod-cone-mediated PLR, as red light of 630 nm wavelength does not activate the intrinsic RGC photopigment melanopsin (Fig. 5). Blue light was used to elicit combined responses (rod-cone response + melanopsin intrinsic response). The wavelength of light emitted by the diodes was 622 ± 7 nm for red light and 463 ± 13 nm for blue light. Red and blue light stimuli were matched and had illuminance of 1 (0 log units), 4 (0.6 log units), 16 (1.2 log units), 63 (1.8 log units), 251 (2.4 log units), and 1000 (3 log units) lux. The maximum luminance measured at the position of the mouse eye using a photometer (J17LumaColor with luminance head model J1803; Tektronix, Wilsonville, OR, USA) was 3700 cd/m^2 for the illuminance of 1000 lux. The pupil was illuminated for a period of 500 ms. All PLR testing routines were recorded in completely awake mouse without the use of general anesthetic or sedation. The mice were initially habituated to extensive handling with food rewards, in order for them to remain calm during recording. The experiments were then carried out under scotopic conditions with no background illumination from the pupillometer. Only the direct response of the pupil was observed following illumination with red/blue light stimulus. The pupil response was expressed as the percent contraction of the pupil from baseline.

To evaluate pupil responses with much higher light intensity, the PLR analysis was performed using a Melan-100 instrument (BioMed Vision Technologies, Ames, IA, USA). Similar as before, mice (n = 11) were awake during the recording session and were held still using minimal manual restraint. Recording sessions in most animals lasted <1 min. The Melan-100 (BioMed Vision Technologies) has two powerful diode-based light sources with very narrow wavelength bands (630 ± 5 nm for red light, luminance 200 kcd/m^2; 475 ± 5 nm for the blue light, luminance 200 kcd/m^2). Baseline pupil diameter measurements in mice were taken in darkness prior to illumination using an infrared video camera (Sony Handycam, Sony Corporation). Red light stimuli with 2-s duration were used to illuminate one eye of the mouse at a distance of 4 cm from the ocular surface, and direct pupil responses were recorded from the illuminated eye with the digital infrared camera. Prior to performing illumination with the blue light, pupils were allowed to completely dilate to the baseline diameter. Captured digital movies of pupil responses were analyzed using ADOBE PHOTOSHOP (v. 10.0.1; Adobe Systems, Inc., San Jose, CA, USA). Calibrated dot grid with dot sizes of 0.5, 1, 1.5, 2, and 3 mm in diameter were recorded with a camera from the 4 cm distance to calculate the regression equation so calculation of absolute pupil diameters from the recorded images could be performed.

Spectral-domain optical coherence tomography

Spectral-domain optical coherence tomography analysis was performed on anesthetized mice (n = 22) using a Spectralis SD-OCT (Heidelberg Engineering, Vista, CA, USA) imaging system (Fig. 1b), coupled with a 25D lens for mouse ocular imaging (Heidelberg Engineering). Mice were anesthetized using 2.5% halothane and 100% oxygen mixture on a heating pad to maintain body temperature. Pupils were dilated using a 1% tropicamide solution. The cornea

was moisturized with a saline solution, which was applied every 20–30 s. Circular scans around the optic nerve region were performed to quantify NFL thickness in the temporal, superior, nasal and inferior retinal quadrants. Circular scans were subsequently analyzed by including or excluding blood vessels from the RNFL thickness calculation, because blood vessels in rodents are almost completely embedded in the RNFL[50] and are included in automated RNFL measurement routines by all commercially available systems. Linear scans were also performed in the superio-temporal region of the retina (*area centralis*) to evaluate total retinal thickness, thickness of the photoreceptor layer, and the RNFL thickness. Total of 25 linear scan lines were positioned in the superio-temporal retina. The most superior linear scan line was positioned 2.5–3 mm superior/1.5–2 mm temporal to the optic nerve head.

Statistical analysis

All statistical analyses were carried out using GRAPHPAD PRISM 5.0 (GraphPad software, San Diego, CA, USA). Paired *t*-tests, one-way ANOVA with Bonferroni's post test, or repeated measures ANOVA with Bonferroni's post test analysis were used as described in the text. Differences between groups were considered statistically significant for $P < 0.05$.

RESULTS

Pattern electroretinography

Average pERG amplitudes were 9 ± 0.6 μV (N35-P50, mean ± SEM) and 11.2 ± 0.7 μV (P50-N95, Fig. 3a). Repeated measurement of pERG amplitudes in the same mice (four different recording sessions with a 7 day time interval between sessions for the same animal) revealed no significant inter-session difference compared with initial baseline recordings ($P = 0.4$, Repeated Measures ANOVA with Bonferroni post test analysis, Fig. 3b). The intraanimal variability across recording sessions was 1.9 ± 0.1 μV, with a 27.1 ± 2.7% coefficient of variation. Additionally, comparison of pERG amplitudes from the right and left eye revealed no significant interocular variability for the N35-P50 ($P = 0.5$, paired *t*-test) or P50-N95 amplitudes ($P = 0.1$, paired *t*-test). The pERG implicit times were 29.3 ± 1.8 ms (N35), 78.4 ± 3.5 ms (P50), and 168.9 ± 6.6 ms (N95), with durations of 49.2 ± 3.2 ms (N35-P50) and 90.4 ± 5.4 ms (P50-N95, Fig. 3c,d). To observe the effect of aging on the pERG response, recordings were conducted at 3, 11, and 15 months of age on the same animals (Fig. 4). The average N35-P50 amplitude was 4.3 ± 0.9, 6.6 ± 1.1, and 6.2 ± 1.4 μV at 3, 11, and 15 months of age, respectively (Fig. 4a). The average P50-N95 amplitude was 8.7 ± 1.3, 7.9 ± 0.5, and 7.9 ± 1 μV at 3, 11, and 15 months of age, respectively (Fig. 4b). The average N35-P50 latency was 42.1 ± 5.3, 58.5 ± 13.2, and 56.7 ± 9.3 ms at 3, 11, and 15 months of age, respectively (Fig. 4c). The average P50-N95 latency was 86 ± 14.3, 137.4 ± 18.1, and 123.9 ± 14.4 ms at 3, 11, and 15 months of age, respectively (Fig. 4d). No statistically significant difference was observed in both amplitudes and latencies at different ages (Repeated Measures ANOVA with Bonferroni post test analysis: N35-P50 amplitude, $P = 0.3$; P50-N95

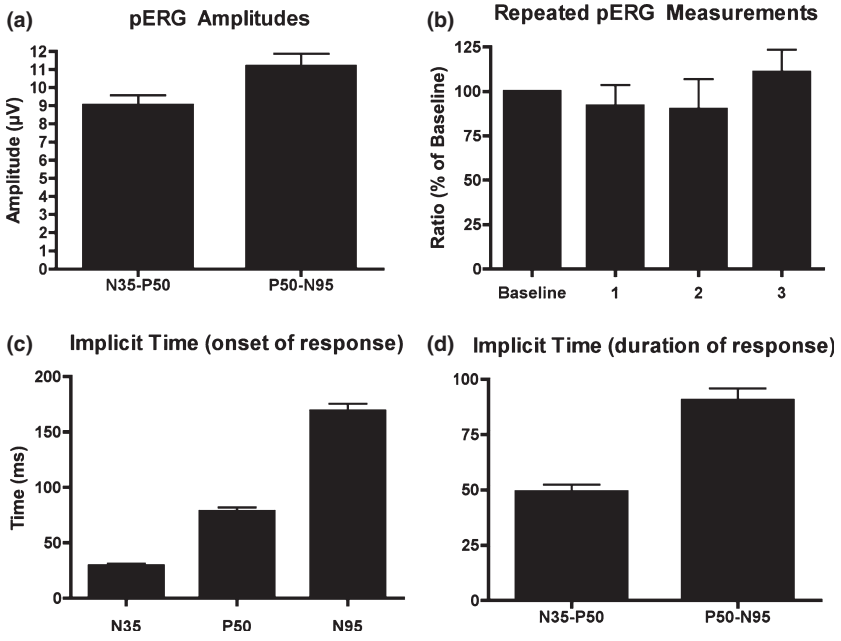

Figure 3. Pattern ERG responses in healthy mice. (a) Average pattern electroretinography (pERG) N35-P50 and P50-N95 amplitudes. (b) Repeated measurement of pERG amplitude (amplitudes are presented as a ratio against the very first recording) in the same mice did not reveal significant differences ($P > 0.1$, Repeated Measures ANOVA). (c, d) Analysis of implicit times showed higher implicit time for specific components of pERG waveform in mice when compared to previously reported values in humans and dogs.

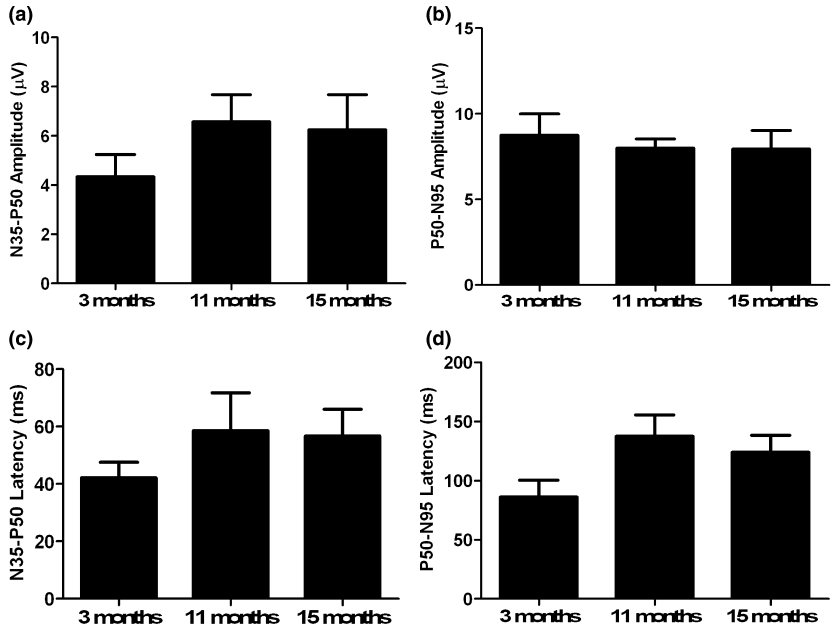

Figure 4. Effect of age on pattern ERG responses in healthy mice. (a–d) There was no statistically significant difference in amplitudes (a, N35-P50 amplitude; b, P50-N95 amplitude) and latencies (c, N35-P50 latency; d, P50-N95 latency) between 3, 11, and 15-month-old mice.

amplitude, $P = 0.8$; N35-P50 latency, $P = 0.5$; and P50-N95 latency, $P = 0.1$).

Chromatic pupillography

The visual pigments present in the mouse retina (Fig. 5) have been previously characterized,[51–53], and their differential contribution to the pupil light reflex has been utilized to characterize the functional properties of different retinal neuronal cells.[24] For red light stimulus, the pupil constriction was 3.3 ± 0.4% of baseline size (0 log units), 6.6 ± 0.7% (0.6 log units), 14 ± 1.2% (1.2 log units), 21.13 ± 1.8% (1.8 log units), 25.9 ± 1.1% (2.4 log units), and 31.6 ± 0.9% (3.0 log units), respectively (Fig. 6). However, blue light stimuli resulted in significantly greater pupil constriction for all tested light intensities (Fig. 6): 0 log units, 20.3 ± 1.8% ($P < 0.0001$, paired *t*-test); 0.6 log units, 30.3 ± 1.5% ($P < 0.0001$, paired *t*-test); 1.2 log units, 42.6 ± 1.7% ($P < 0.0001$, paired *t*-test); 1.8 log units, 51 ± 2% ($P = 0.0001$, paired *t*-test); 2.4 log units, 60.6 ± 2.9% ($P < 0.0001$, paired *t*-test); and 3.0 log units, 64 ± 3% ($P < 0.0001$, paired *t*-test).

Pupil constriction in response to light of different wavelengths was also characterized with the Melan-100 instrument (BioMed Vision Technologies) using higher light intensity (200 kcd/m^2). Baseline pupil diameters calculated prior to illumination in dim light conditions were 2.1 ± 0.05 mm (Fig. 7a,d). The pupil diameter after constriction in response to red (630 nm) light stimulation was 1.1 ± 0.05 mm (Fig. 7b,d). Stimulation with blue light induced significantly greater constriction of the pupil to a diameter of 0.56 ± 0.03 mm, compared with stimulation with red light (Fig. 7c,d; $P < 0.001$, paired *t*-test). The pupil

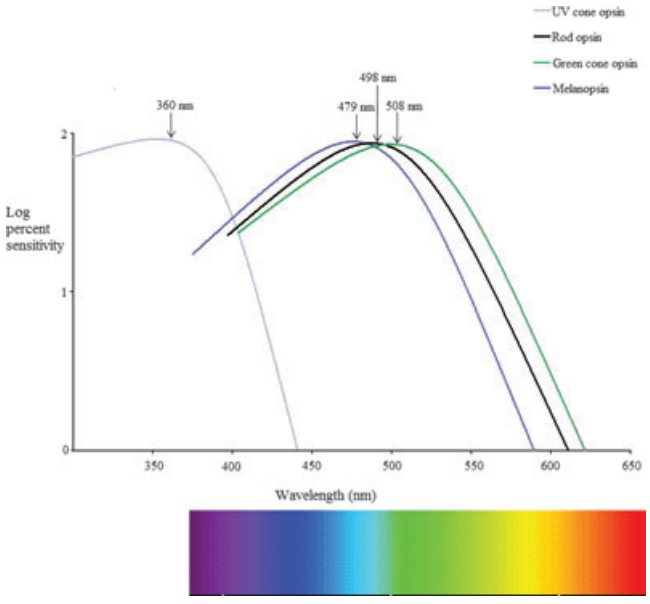

Figure 5. Spectral properties of visual pigments in mice. Mouse retina has following visual pigments: rod opsin (λ_{max} at 498 nm), and two cone opsins (the UV cones with λ_{max} at 360 nm and the green cones with λ_{max} at 508 nm). In addition to these photoreceptor pigments, a specific subset of ganglion cells (intrinsically photosensitive retinal ganglion cells = ipRGC) contains the photopigment melanopsin, which has λ_{max} at 479 nm. Therefore, when red light of 620–630 nm wavelength is used as a stimulus, only the green cones and rods are activated. However, when blue light of wavelength 480 nm is directed on the retina, all retinal photopigments (with exception of UV cones) are activated. This difference in spectral properties can be utilized to identify functional deficits in specific cell types within the retina (Figure modified from Lucas, Douglas *et al.* 2001).

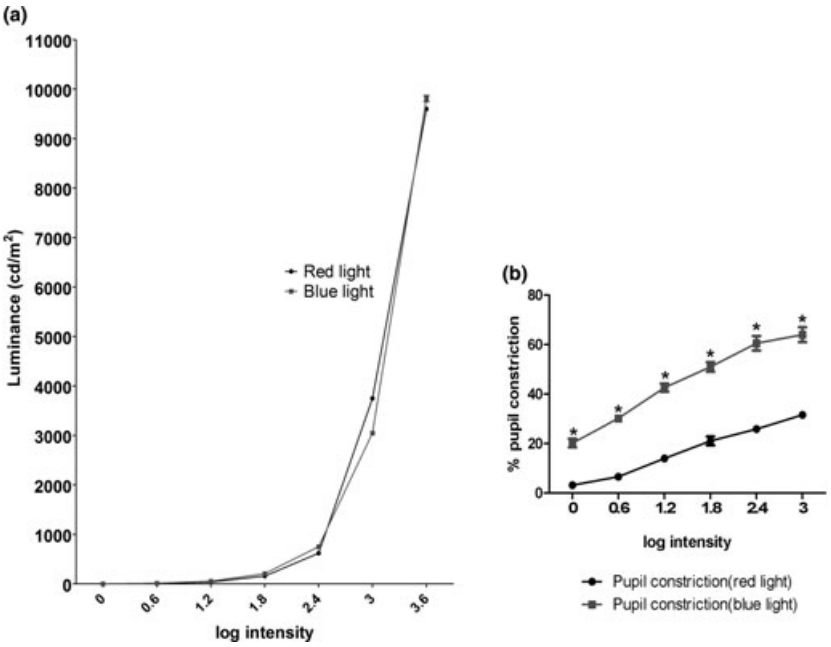

Figure 6. Chromatic pupil light reflex evaluation in mice using A-2000. (a) Luminance of red and blue lights for different illumination parameters (0, 0.6, 1.2, 1.8, 2.4, 3 log (lux) units) was measured using a photometer. (b) Significantly higher pupil constriction was observed following blue light stimulus when compared to the red light stimulus for all tested light intensities (*$P < 0.0001$).

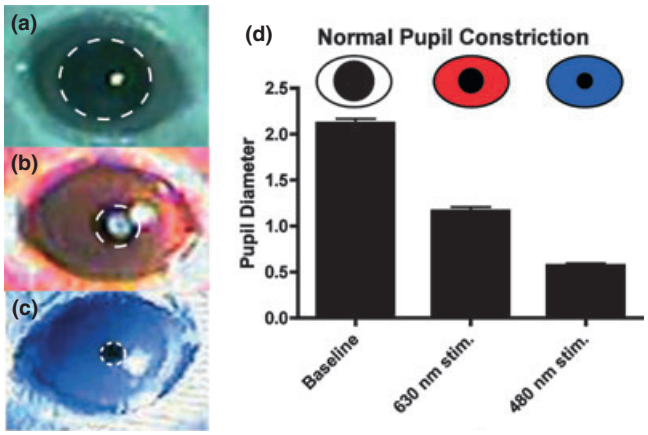

Figure 7. Chromatic pupil light reflex in mice using Melan-100 (Bio-Med Vision Technologies). Representative images of pupil (a) baseline diameter, and after stimulation with (b) red (630 nm, 200 kcd/m^2) or (c) blue (480 nm, 200 kcd/m^2) light. (d) Pupil diameter variation from baseline following stimulation with red and blue light.

constricted by 44.3 ± 3.3% (mean ± SEM) of the baseline value with red light stimulus, and the pupil constricted by 71.8 ± 1.9% of the baseline value with blue light stimulus.

Optical coherence tomography

Spectral-domain OCT was used to noninvasively analyze the RNFL and total retinal thickness *in vivo*. Spectral-domain optical coherence tomography analysis revealed a total retinal thickness of 229.5 ± 1.7 μm (Figs 8a,9a; mean ± SEM) in the *area centralis* of healthy mouse eyes. The photoreceptor layer thickness was 83.8 ± 0.7 μm, with RNFL thickness of 29 ± 0.5 μm in the region of the retina that corresponds to the *area centralis* (Figs 8a,9a). The thickness of the RNFL using circular scans and automated segmentation protocols was 46.7 ± 0.9 μm (temporal), 46.1 ± 0.9 μm (superior), 45.8 ± 0.9 μm (nasal), and 48.4 ± 1 μm (inferior) (Figs 8,9). The thickness of the RNFL did not vary between quadrants ($P = 0.1$, ANOVA with Bonferroni's post test). Analysis of RNFL thickness by excluding blood vessels thickness from the calculation was 22.8 ± 0.6 μm (temporal), 24.4 ± 0.5 μm (superior), 24.3 ± 0.6 μm (nasal), and 23.6 ± 0.8 μm (inferior) (Figs 8b,9c). The thickness of the RNFL did not vary between quadrants ($P = 0.2$, ANOVA with Bonferroni's post test). Exclusion of blood vessels from the analysis resulted in significantly decreased RNFL thickness for all tested quadrants when compared to values obtained with inclusion of blood vessels: temporal ($P < 0.0001$, paired *t*-test), superior ($P < 0.0001$), nasal ($P < 0.0001$), and inferior quadrant ($P < 0.0001$).

DISCUSSION

Repeated measurements of RGC structural and functional parameters are essential for following temporal disease progression or treatment effectiveness in different models of retina and optic nerve diseases. In this study, we have characterized the normative values for healthy adult C57BL/6 mice using pERG, chromatic pupillography and OCT.

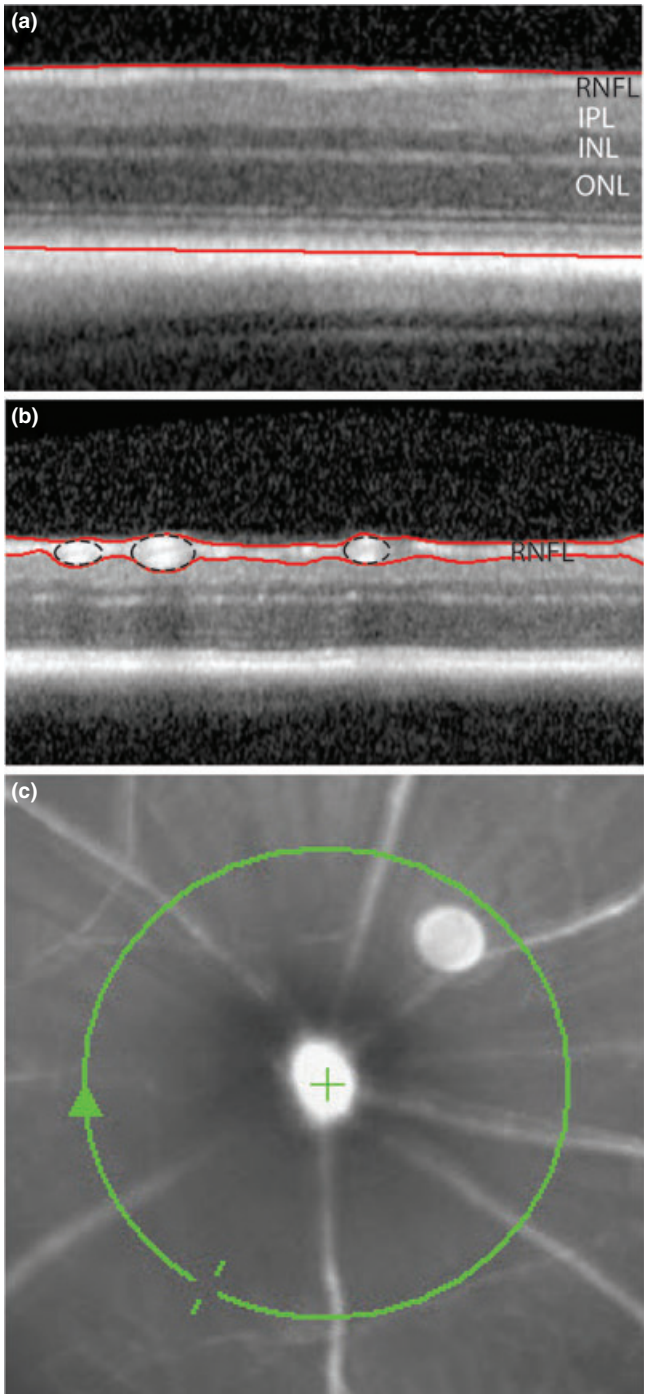

Figure 8. Optical coherence tomography. (a) Retina linear scans were used to evaluate the total retinal thickness and to calculate the thickness of the outer nuclear layer (photoreceptor bodies) and the RNFL in the superior retina (*area centralis* region). (b) Peripapillary scans were used to determine the RNFL thickness in the temporal, superior, nasal, and inferior retinal quadrants. Area of blood vessels is demarcated with dashed circles. (c) Fundus image of a mouse eye demonstrating area of the circular scan (gray circle). RNFL = retinal nerve fiber layer; IPL = inner plexiform layer; INL = inner nuclear layer; ONL = outer nuclear layer.

Pattern electroretinography has been successfully used in a rodent model of hereditary glaucoma (DBA/2J) to detect RGC deficits.[54] The baseline values reported for young DBA/2J mice prior to loss of RGCs were 8.15 ± 0.4 μV, which are similar to values obtained from adult healthy mice in our study. Repeatability is particularly important if pERG is to be used as a longitudinal tool to monitor RGC function for comparative purposes during disease progression or treatment effectiveness in the same animal. We have demonstrated that pERG recordings did not have significant inter-session differences from baseline in our experimental conditions. The lateral eye position of rodents necessitates recording either one eye at a time or using two different stimulus monitors simultaneously; in our study, we have recorded one eye at a time using a single stimulus monitor, similar to previously published studies.[54,55] The experimental setup that we used did not result in a significant interocular difference of pERG amplitudes or implicit times between right and left eyes, providing an opportunity to effectively monitor temporal RGC function in each eye. Furthermore, we have demonstrated that the RGC function does not vary significantly as mice age from 3 to 15 months. The pERG amplitudes and latencies at 11 and 15 months of age did not change significantly from earlier recordings on the same mice at 3 months of age.

The PLR is an objective measure of retina and optic nerve function. The PLR has been used to monitor functional deficits caused by retina and optic nerve diseases in laboratory animals.[1,2,56–58] Recently, chromatic PLR analysis has been used in clinical settings in humans[59–61] and dogs[24] to monitor the rod-cone-mediated and melanopsin-mediated PLR responses. White light has been traditionally used for PLR analysis both clinically and experimentally. As white light is a mixture of wavelengths of the visible spectrum (including red and blue), differentiation of rod-cone and ipRGC-mediated PLR activity cannot effectively be achieved with white light stimuli. As previously shown in healthy dogs,[24] we have demonstrated that red light causes significantly less pupil constriction when compared to the blue light stimulation in healthy mouse eyes. As blue light of 480 nm wavelength can activate all visual pigments in the mouse retina except the UV cone opsin, this type of stimulus provides the most robust activation of the PLR response. Based on the spectral properties of photosensitive pigments in mice, the red light (630 nm) can activate rhodopsin and M cones, but not UV cones and the intrinsic photosensitive pigment melanopsin,[62,63] which provides an opportunity for the specific evaluation of rod-cone-mediated functional properties by measuring the red light-mediated PLR responses. It has been previously shown that the ipRGCs project to midbrain structures and can mediate PLR activity and photopic blink response even in the complete absence of rod-cone input.[64] Furthermore, a subset of ipRGCs project to the region of the lateral

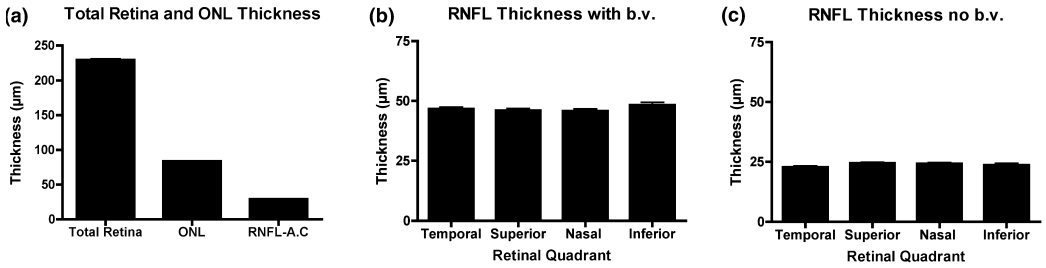

Figure 9. Spectral-domain optical coherence tomography (SD-OCT) retinal thickness parameters in healthy mice. (a) Total retinal thickness, photoreceptor layer thickness, and retinal nerve fiber layer (RNFL) thickness at the *area centralis* region, measured using SD-OCT. (b) Circular scan analysis of the RNFL thickness with inclusion of blood vessels in the RNFL profile—there was no significant difference in RNFL thickness in different quadrants. (c) Circular scan analysis of the RNFL thickness without inclusion of blood vessels in the RNFL profile showed significantly smaller thickness compared with values obtained by calculations performed by standard software routines (with inclusion of blood vessels) presented in image b. ONL = outer nuclear layer, AC = area centralis, b.v. = blood vessel.

geniculate nucleus (LGN) and can mediate irradiance dependent firing rates of almost 40% of neurons in the LGN.[65] While the small number of ipRGCs in the mammalian retina does not suggest a primary role of ipRGCs in visual processing, a recent study has demonstrated that rod and cone deficient mice can still effectively recognize pattern gratings in a visual maze test using only melanopsin-mediated light processing.[66] Because the peak of melanopsin activation occurs near 480 nm (blue light)[62] and melanopsin cannot be activated by red light (630 nm), red light-based routines for evaluation of PLR can be effectively used to evaluate the status of RGC dendritic synaptic connections in cases where the rod and cone electrical activity is completely normal. A defect in the red light pupil response (rod-cone-mediated signaling to ipRGCs) coupled with a normal blue light pupil response (suggestive of the normal ipRGC function) and normal scotopic and photopic ERG responses could be potentially indicative of a dysfunction in the RGC dendritic network. Chromatic PLR evaluation could be used for monitoring early retinal functional deficits in transgenic mouse models, or as an objective test for evaluation of the retina and RGC function as a result of experimental therapeutic treatments. Defects of the pupillary light reflex after illumination with the red and blue light in the presence of normal scotopic and photopic ERG responses would indicate a problem with the ipRGC soma, axons, or higher processing areas of the brain (pretectum) or more distal nerve or iris muscle deficits. Considering that rod-cone-mediated pupil input has to converge to ipRGCs that have large diameter axons, compressive optic nerve lesions and inflammatory optic nerve conditions theoretically could selectively impair this cell population resulting in decreased or absent PLR response while still sparing majority (or some) of smaller diameter RGCs resulting in the presence of some functional vision (Grozdanic *et al.*, ACVO Abstract, San Antonio, TX, 2006). However, a majority of clinical and experimental conditions that we have evaluated during the last 5 years using chromatic PLR testing in different animal species are frequently characterized by an intact ipRGC-mediated response to blue light illumination—even in cases where complete blindness based on visual behavior is already present.[24]

While pERG and PLR are functional monitoring techniques that can detect functional deficits before any structural retina or RNFL changes occur, observation of structural retina parameters remains a very frequently utilized measure of therapeutic outcome in animal models of ophthalmic diseases. Spectral-domain OCT is a tool that has been extensively used to diagnose and monitor diseases of the eye and retina including glaucoma,[67] retinitis pigmentosa,[68] and macular degeneration.[69] Measurements of macular volume[70] and RNFL thickness[71] using OCT have also been used to estimate overall neuronal loss in patients with multiple sclerosis, while one recent clinical study has demonstrated inner retina thinning in patients with idiopathic Parkinson's disease.[72] Considering the diversity of transgenic mouse models for ophthalmic and neurodegenerative diseases, it is likely that SD-OCT imaging will become a useful technique for evaluation of structural optic nerve properties in many different animal disease models. Similar to recently published results with the use of adaptive optics and 78D lens,[73] we have demonstrated that by using a 25-diopter lens, high quality OCT scans of the mouse retina can be obtained. It has been previously demonstrated that automated RNFL analysis routines overestimate RNFL thickness because of the inclusion of blood vessels in the RNFL thickness calculation.[74] We have also demonstrated a substantial increase in the RNFL thickness when blood vessels were included in the calculation. As blood vessels are predominately embedded within the RNFL in a majority of animal species, a subtle increase or decrease in RNFL thickness could be potentially masked by change in the blood vessel diameter because of the overwhelming contribution of the blood vessels to the RNFL thickness calculations with conventional SD-OCT software.

There are several limitations which can decrease the effective use of the cPLR and SD-OCT responses for evaluation

of the retina and optic nerve status. Mice with severe forms of iris atrophy or prominent intraocular inflammation can have significantly attenuated PLR responses, while the application of topical ocular medications with miotic or mydriatic action can also have a significant effect on the resting pupil diameter and overall pupil motility. Furthermore, CNS and peripheral nerve abnormalities, which can be frequently present in different transgenic mouse models affecting any of the subthalamic PLR centers or efferent PLR pathway components, can have significant effects on the quality of PLR responses, which may be a potentially limiting factor during cPLR testing routines. Similarly, limitations in pupil dilatation may have the potential effect on the quality of SD-OCT imaging. Presently, we are developing automated OCT segmentation software routines that are specific for mouse retina which are likely to improve further the application of OCT in mouse species.

Detailed *in vivo* analysis of functional and structural retina and RGC parameters can provide a significant advantage during evaluation of transgenic animal models of human ocular and neurodegenerative diseases. Introduction of these techniques may result in a significant acceleration developing new therapeutic strategies, because all observed techniques are commonly utilized in human patients, which may allow for a rapid translation of animal study results to human patient population. Considering that the mouse is probably the most frequent experimental animal species encountered by veterinary ophthalmologists during toxicity and clinical safety/efficacy studies, the availability of normative pERG, chromatic PLR, and OCT data may provide useful information for more specific evaluation of functional and structural retinal properties in this particular animal species.

ACKNOWLEDGMENTS

This work was supported by the Department of Veterans Affairs Center for Prevention and Treatment of Vision Loss (CPTVL), VA RRD Grants C3919R and C4702R, Iowa Center for Advanced Neurotoxicology (ICAN), and the NIH (1R01EY019294).

REFERENCES

1. Grozdanic S, Betts DM, Allbaugh RA *et al.* Characterization of the pupil light reflex, electroretinogram and tonometric parameters in healthy mouse eyes. *Current Eye Research* 2003; **26**: 371–378.
2. Grozdanic S, Sakaguchi DS, Kwon YH *et al.* Characterization of the pupil light reflex, electroretinogram and tonometric parameters in healthy rat eyes. *Current Eye Research* 2002; **25**: 69–78.
3. Grozdanic SD, Matic M, Betts DM *et al.* Recovery of canine retina and optic nerve function after acute elevation of intraocular pressure: implications for canine glaucoma treatment. *Veterinary Ophthalmology* 2007; **10**(Suppl. 1): 101–107.
4. Panagakis E, Moschos M. Pattern ERG changes in suspected glaucoma. *Ophthalmologica* 1998; **212**: 112–114.
5. Mierdel P, Zenker HJ, Marre E. The pattern ERG in glaucoma: effect of pattern reversal time. *International Ophthalmology* 1992; **16**: 211–214.
6. Price MJ, Drance SM, Price M *et al.* The pattern electroretinogram and visual-evoked potential in glaucoma. *Graefes Archive for Clinical and Experimental Ophthalmology* 1988; **226**: 542–547.
7. van den Berg TJ, Riemslag FC, de Vos GW *et al.* Pattern ERG and glaucomatous visual field defects. *Documenta Ophthalmologica* 1986; **61**: 335–341.
8. Papst N, Bopp M, Schnaudigel OE. Pattern electroretinogram and visually evoked cortical potentials in glaucoma. *Graefes Archive for Clinical and Experimental Ophthalmology* 1984; **222**: 29–33.
9. Wanger P, Persson HE. Pattern-reversal electroretinograms in unilateral glaucoma. *Investigative Ophthalmology & Visual Science* 1983; **24**: 749–753.
10. Porciatti V, Nagaraju M. Head-up tilt lowers IOP and improves RGC dysfunction in glaucomatous DBA/2J mice. *Experimental Eye Research* 2010; **90**: 452–460.
11. Nagaraju M, Saleh M, Porciatti V. IOP-dependent retinal ganglion cell dysfunction in glaucomatous DBA/2J mice. *Investigative Ophthalmology & Visual Science* 2007; **48**: 4573–4579.
12. Porciatti V. The mouse pattern electroretinogram. *Documenta Ophthalmologica* 2007; **115**: 145–153.
13. Viswanathan S, Frishman LJ, Robson JG. The uniform field and pattern ERG in macaques with experimental glaucoma: removal of spiking activity. *Investigative Ophthalmology & Visual Science* 2000; **41**: 2797–2810.
14. Miura G, Wang MH, Ivers KM *et al.* Retinal pathway origins of the pattern ERG of the mouse. *Experimental Eye Research* 2009; **89**: 49–62.
15. Porciatti V, Ventura LM. Adaptive changes of inner retina function in response to sustained pattern stimulation. *Vision Research* 2009; **49**: 505–513.
16. Maffei L, Fiorentini A, Bisti S *et al.* Pattern ERG in the monkey after section of the optic nerve. *Experimental Brain Research* 1985; **59**: 423–425.
17. Mafei L, Fiorentini A. Electroretinographic responses to alternating gratings before and after section of the optic nerve. *Science* 1981; **211**: 953–955.
18. Hull BM, Thompson DA. A review of the clinical applications of the pattern electroretinogram. *Ophthalmic & Physiological Optics: The Journal of the British College of Ophthalmic Opticians* 1989; **9**: 143–152.
19. Bach M. Electrophysiological approaches for early detection of glaucoma. *European Journal of Ophthalmology* 2001; **11**(Suppl. 2): S41–S49.
20. Ventura LM, Porciatti V. Pattern electroretinogram in glaucoma. *Current Opinion in Ophthalmology* 2006; **17**: 196–202.
21. Ben-Shlomo G, Bakalash S, Lambrou GN *et al.* Pattern electroretinography in a rat model of ocular hypertension: functional evidence for early detection of inner retinal damage. *Experimental Eye Research* 2005; **81**: 340–349.
22. Grozdanic S, Kecova H, Harper MM *et al.* Functional and structural changes in a canine model of hereditary primary angle-closure glaucoma. *Investigative Ophthalmology & Visual Science* 2010; **51**: 255–263.
23. Ofri R, Samuelson DA, Strubbe DT *et al.* Altered retinal recovery and optic nerve fiber loss in primary open-angle glaucoma in the beagle. *Experimental Eye Research* 1994; **58**: 245–248.
24. Grozdanic SD, Matic M, Sakaguchi DS *et al.* Evaluation of retinal status using chromatic pupil light reflex activity in healthy and diseased canine eyes. *Investigative Ophthalmology & Visual Science* 2007; **48**: 5178–5183.

25. Kardon R, Anderson SC, Damarjian TG *et al.* Chromatic pupil responses: preferential activation of the melanopsin-mediated versus outer photoreceptor-mediated pupil light reflex. *Ophthalmology* 0161-6420 2009; **116**: 1564–1573.
26. Park JC, Moura AL, Raza AS *et al.* Toward a clinical protocol for assessing rod, cone, and melanopsin contributions to the human pupil response. *Investigative Ophthalmology & Visual Science* 2011; **52**: 6624–6635.
27. McDougal DH, Gamlin PD. The influence of intrinsically-photosensitive retinal ganglion cells on the spectral sensitivity and response dynamics of the human pupillary light reflex. *Vision Research* 2010; **50**: 72–87.
28. McNeill DS, Sheely CJ, Ecker JL *et al.* Development of melanopsin-based irradiance detecting circuitry. *Neural Development* 2011; **6**: 8.
29. Tsujimura S, Ukai K, Ohama D *et al.* Contribution of human melanopsin retinal ganglion cells to steady-state pupil responses. *Proceedings Biological Sciences/The Royal Society* 2010; **277**: 2485–2492.
30. Tsujimura S, Tokuda Y. Delayed response of human melanopsin retinal ganglion cells on the pupillary light reflex. *Ophthalmic & Physiological Optics: The Journal of The British College of Ophthalmic Opticians* 2011; **31**: 469–479.
31. Benarroch EE. The melanopsin system: phototransduction, projections, functions, and clinical implications. *Neurology* 2011; **76**: 1422–1427.
32. Markwell EL, Feigl B, Zele AJ. Intrinsically photosensitive melanopsin retinal ganglion cell contributions to the pupillary light reflex and circadian rhythm. *Clinical & Experimental Optometry: Journal of the Australian Optometrical Association* 2010; **93**: 137–149.
33. Do MT, Yau KW. Intrinsically photosensitive retinal ganglion cells. *Physiological Reviews* 2010; **90**: 1547–1581.
34. Schmidt TM, Kofuji P. Novel insights into non-image forming visual processing in the retina. *Cellscience* 2008; **5**: 77–83.
35. Grozdanic SD, Harper MM, Kecova H. Antibody-mediated retinopathies in canine patients: mechanism, diagnosis, and treatment modalities. *The Veterinary Clinics of North America. Small Animal Practice* 2008; **38**: 361–387. vii.
36. Kankipati L, Girkin CA, Gamlin PD. Post-illumination pupil response in subjects without ocular disease. *Investigative Ophthalmology & Visual Science* 2010; **51**: 2764–2769.
37. Zele AJ, Feigl B, Smith SS *et al.* The circadian response of intrinsically photosensitive retinal ganglion cells. *PLoS One* 2011; **6**: e17860.
38. Kocaoglu OP, Uhlhorn SR, Hernandez E *et al.* Simultaneous fundus imaging and optical coherence tomography of the mouse retina. *Investigative Ophthalmology & Visual Science* 2007; **48**: 1283–1289.
39. Fingler J, Readhead C, Schwartz DM *et al.* Phase-contrast OCT imaging of transverse flows in the mouse retina and choroid. *Investigative Ophthalmology & Visual Science* 2008; **49**: 5055–5059.
40. Srinivasan VJ, Ko TH, Wojtkowski M *et al.* Noninvasive volumetric imaging and morphometry of the rodent retina with high-speed, ultrahigh-resolution optical coherence tomography. *Investigative Ophthalmology & Visual Science* 2006; **47**: 5522–5528.
41. Strouthidis NG, Grimm J, Williams GA *et al.* A comparison of optic nerve head morphology viewed by spectral domain optical coherence tomography and by serial histology. *Investigative Ophthalmology & Visual Science* 2009; **29**: 29.
42. Wang M, Hood DC, Cho JS *et al.* Measurement of local retinal ganglion cell layer thickness in patients with glaucoma using frequency-domain optical coherence tomography. *Archives of Ophthalmology* 2009; **127**: 875–881.
43. Abramoff MD, Lee K, Niemeijer M *et al.* Automated segmentation of the cup and rim from spectral domain OCT of the optic nerve head. *Investigative Ophthalmology & Visual Science* 2009; **50**: 5778–5784.
44. Garvin MK, Abramoff MD, Kardon R *et al.* Intraretinal layer segmentation of macular optical coherence tomography images using optimal 3-D graph search. *IEEE Transactions on Medical Imaging* 2008; **27**: 1495–1505.
45. Kim KH, Puoris'haag M, Maguluri GN *et al.* Monitoring mouse retinal degeneration with high-resolution spectral-domain optical coherence tomography. *Journal of Vision* 2008; **8**: 17–11.
46. Xu J, Molday LL, Molday RS *et al.* In vivo imaging of the mouse model of X-linked juvenile retinoschisis with fourier domain optical coherence tomography. *Investigative Ophthalmology & Visual Science* 2009; **50**: 2989–2993.
47. Cebulla CM, Ruggeri M, Murray TG *et al.* Spectral domain optical coherence tomography in a murine retinal detachment model. *Experimental Eye Research* 2010; **90**: 521–527.
48. Huber G, Beck SC, Grimm C *et al.* Spectral domain optical coherence tomography in mouse models of retinal degeneration. *Investigative Ophthalmology & Visual Science* 2009; **50**: 5888–5895.
49. Sho K, Takahashi K, Fukuchi T *et al.* Quantitative evaluation of ischemia-reperfusion injury by optical coherence tomography in the rat retina. *Japanese Journal of Ophthalmology* 2005; **49**: 109–113.
50. Connolly SE, Hores TA, Smith LE *et al.* Characterization of vascular development in the mouse retina. *Microvascular Research* 1988; **36**: 275–290.
51. Bowes C, Li T, Danciger M *et al.* Retinal degeneration in the rd mouse is caused by a defect in the beta subunit of rod cGMP-phosphodiesterase. *Nature* 1990; **347**: 677–680.
52. Lucas RJ, Douglas RH, Foster RG. Characterization of an ocular photopigment capable of driving pupillary constriction in mice. *Nature Neuroscience* 2001; **4**: 621–626.
53. Sun H, Macke JP, Nathans J. Mechanisms of spectral tuning in the mouse green cone pigment. *Proceedings of the National Academy of Sciences of the United States of America* 1997; **94**: 8860–8865.
54. Porciatti V, Saleh M, Nagaraju M. The pattern electroretinogram as a tool to monitor progressive retinal ganglion cell dysfunction in the DBA/2J mouse model of glaucoma. *Investigative Ophthalmology & Visual Science* 2007; **48**: 745–751.
55. Ben-Shlomo G, Ofri R. Development of inner retinal function, evidenced by the pattern electroretinogram, in the rat. *Experimental Eye Research* 2006; **83**: 417–423.
56. Trejo LJ, Cicerone CM. Retinal sensitivity measured by the pupillary light reflex in RCS and albino rats. *Vision Research* 1982; **22**: 1163–1171.
57. Aleman TS, Jacobson SG, Chico JD *et al.* Impairment of the transient pupillary light reflex in Rpe65(-/-) mice and humans with leber congenital amaurosis. *Investigative Ophthalmology & Visual Science* 2004; **45**: 1259–1271.
58. Whiteley SJ, Young MJ, Litchfield TM *et al.* Changes in the pupillary light reflex of pigmented royal college of surgeons rats with age. *Experimental Eye Research* 1998; **66**: 719–730.
59. Kardon R, Anderson SC, Damarjian TG *et al.* Chromatic pupillometry in patients with retinitis pigmentosa. *Ophthalmology* 2011; **118**: 376–381.
60. de Zavalia N, Plano SA, Fernandez DC *et al.* Effect of experimental glaucoma on the non-image forming visual system. *Journal of Neurochemistry* 2011; **117**: 904–914.
61. Kankipati L, Girkin CA, Gamlin PD. The post-illumination pupil response is reduced in glaucoma patients. *Investigative Ophthalmology & Visual Science* 2011; **52**: 2287–2292.

62. Hattar S, Lucas RJ, Mrosovsky N *et al.* Melanopsin and rod-cone photoreceptive systems account for all major accessory visual functions in mice. *Nature* 2003; **424**: 76–81.
63. Fu Y, Zhong H, Wang M-HH *et al.* Intrinsically photosensitive retinal ganglion cells detect light with a vitamin A-based photopigment, melanopsin. *Proceedings of the National Academy of Sciences of the United States of America* 2005; **102**: 10339–10344.
64. Hattar S, Kumar M, Park A *et al.* Central projections of melanopsin-expressing retinal ganglion cells in the mouse. *The Journal of Comparative Neurology* 2006; **497**: 326–349.
65. Brown TM, Wynne J, Piggins HD *et al.* Multiple hypothalamic cell populations encoding distinct visual information. *Journal of Physiology* 2011; **589**: 1173–1194.
66. Ecker JL, Dumitrescu ON, Wong KY *et al.* Melanopsin-expressing retinal ganglion-cell photoreceptors: cellular diversity and role in pattern vision. *Neuron* 2010; **67**: 49–60.
67. Forte R, Ambrosio L, Bonavolonta P *et al.* Pattern electroretinogram optimized for glaucoma screening (PERGLA) and retinal nerve fiber thickness in suspected glaucoma and ocular hypertension. *Documenta Ophthalmologica* 2010; **120**: 187–192.
68. Huang Q, Chowdhury V, Coroneo MT. Evaluation of patient suitability for a retinal prosthesis using structural and functional tests of inner retinal integrity. *Journal of Neural Engineering* 2009; **6**: 035010.
69. Freeman SR, Kozak I, Cheng L *et al.* Optical coherence tomography-raster scanning and manual segmentation in determining drusen volume in age-related macular degeneration. *Retina* 2010; **30**: 431–435.
70. Burkholder BM, Osborne B, Loguidice MJ *et al.* Macular volume determined by optical coherence tomography as a measure of neuronal loss in multiple sclerosis. *Archives of Neurology* 2009; **66**: 1366–1372.
71. Garcia-Martin E, Pueyo V, Martin J *et al.* Progressive changes in the retinal nerve fiber layer in patients with multiple sclerosis. *European Journal of Ophthalmology* 2010; **20**: 167–173.
72. Hajee ME, March WF, Lazzaro DR *et al.* Inner retinal layer thinning in Parkinson disease. *Archives of Ophthalmology* 2009; **127**: 737–741.
73. Fischer MD, Huber G, Beck SC *et al.* Noninvasive, in vivo assessment of mouse retinal structure using optical coherence tomography. *PLoS One* 2009; **4**: e7507.
74. Hood DC, Salant JA, Arthur SN *et al.* The location of the inferior and superior temporal blood vessels and interindividual variability of the retinal nerve fiber layer thickness. *Journal of Glaucoma* 2010; **19**: 158–166.